Electronic Supplementary Information for

Fractal Aggregation and Disaggregation of Newly Formed Iron(III) (Hydr)oxide Nanoparticles in the Presence of Natural Organic Matter and Arsenic

Chelsea W. Neil[1,†], Jessica Ray[1,#], Byeongdu Lee,[2] and Young-Shin Jun[1,*]

[1]*Department of Energy, Environmental & Chemical Engineering,*

Washington University in St. Louis, St. Louis, MO 63130

[2]*X-ray Science Division, Argonne National Laboratory,*

Argonne, IL 60439

Address: One Brookings Drive, Campus Box 1180

E-mail: ysjun@seas.wustl.edu

http://encl.engineering.wustl.edu/

Submitted: December 2015

Revised: March 2016

Environmental Science: Nano

*To Whom Correspondence Should be Addressed

†Current address: Office of Research and Development, National Risk Management Research Laboratory, U.S. Environmental Protection Agency, Cincinnati, Ohio 45268, United States

[#]Current address: Civil & Environmental Engineering, University of California, Berkeley, California 94720, United States

Summary

13 pages, including experimental descriptions, 2 tables and 5 figures

S1. Materials and Sample Preparation

Preparation of Suwannee River natural organic matter (SRNOM) stock solution. To create SRNOM stock solutions, 100 mg of NOM was added to 200 mL of DI water and stirred overnight in the dark. The pH of the solution was adjusted to 8.5 before being vacuum-filtered (VWR Vacuum Filtration System with 0.2 μm PES-membrane). The SRNOM stock solution was refrigerated prior to experimentation and NPOC concentrations were measured using a total organic carbon (TOC) Analyzer (Shimadzu Corporation, Kyoto, Japan). The stock solution was then used to create solutions with NPOC concentrations of 1.5 mg/L for use in experiments.

Zeta potential measurement on quartz powder. While zeta potential measurements for the quartz single surface can be different than the quartz powder, surface charge measurement of the single crystal surface is difficult. Therefore, a few assumptions were made for the quartz powder system. First, the ratio of surface area to solution is not controlled for zeta potential measurements. A very small mass of quartz (< 0.5 g) was added to a relatively large volume of solution (50 mL). The exposed surface area of quartz in our GISAXS reactor is also small relative to the volume of solution. Thus, for both systems, the concentration of iron and other reactants are similar in trend and will be in excess with respect to the given quartz surface area.

Second, regarding the comparison between powder and the single crystal surface, there can be some differences because the quartz powder exposes a variety of crystal surfaces, rather than just the (110) single crystal surface. In our previous publications, the crystal surface used for the iron(III) (hydr)oxide system has not been shown to impact the secondary mineral precipitate phase.[1, 2] Thus, we do not expect that there will be a significant different in the zeta potential trends for the single crystal surface versus the powder.

S2. GISAXS experimental set-up and data analysis.

A *q* range calibration was done using a silver behenate standard prior to conducting GISAXS experiments. While scanning samples during GISAXS, incident X-ray beams are used to graze the substrate surface, scattering X-ray beams, which are then collected by a 2-D detector. The angle of this X-ray beam, e.g. the incidence angle (α_i), is fixed to be 0.11° in order to achieve a reflectivity of 98% using the substrate structure (quartz, SiO_2) and beam energy (14 keV). Therefore, for the 0.11° angle, the scattering of the X-ray beam will mainly result from nanoparticles forming on the quartz substrate surface. In order to analyze this data, the 2-D X-ray scattering patterns are processed by cutting the data along the Yoneda wing. Data processing was accomplished with the GISAXSshop macro, available at APS beamline 12-ID-B. More information on the data reduction procedure can be found in our previous publication.[3]

In order to calculate the heterogeneous nanoparticle size, the time-resolved scattering curves (I(q)) were fit using the following relationship:[4]

$$I(q) = I_0 P_0(q, r_0, \sigma_0) S(q, I_{0s}, d, R_h, v_f), \quad S(1)$$

where P(q, R, σ) is the form factor. For our systems, we used a polydisperse sphere model with the Schultz size distribution because the scattering curves displayed a broad size distribution and lacked form factor oscillations.

Within equation S(1), the structure factor is shown as $S(q, I_{0s}, d, R_h, v_f)$. The structure factor can be broken into two parts as follows for a system containing large aggregates which are composed of smaller primary particles:

$$S(q, I_{0s}, d, R_h, v_f) = I_{0s} q^{-d} + S(q, R_h, v_f), \quad S(2)$$

where, $I_{0s} q^{-d}$ is the Porod scattering from the aggregates. Within this equation, I_{0s} is a scaling constant, d is the Porod power-law exponent (e.g., the fractal dimension), and $S(q, R_h, v_f)$ is the

structure factor for primary particles which comprise infinitely large aggregates. The structure factor here used the hard-sphere Percus-Yevick model, where R_h is the hard-sphere interaction radius and v_f is the volume fraction.[4] The fitting is accomplished using a MATLAB macro, where the user inputs initial values for variables such as I_0, r_0, σ_0, etc. These values are then optimized for fit by the macro and the output is used to calculate R_g.

The fractal dimension was also analyzed at ten minute intervals over the 1 hour reaction period, but it did not change over the reaction period (Table S2).

The primary particle size and relative primary particle volume calculated from fitting the GISAXS 1D scattering patterns was consistent between experiments during different beamtimes. The fitting of the primary particles is included in the form factor, P(q). This factor does not include the scattering from aggregates of the primary particles, which is fitted with a power law scattering included in the structure factor, S(q).

S3. Ex situ *precipitate physicochemical characteristics*

Fourier transform infrared spectroscopy (FTIR). FTIR results (Figure S4) give more detailed chemical bonding nature of what is occurring in the Fe + NOM and Fe + As + NOM systems. NOM-containing systems had a double peak around 1600–1700 cm^{-1}.[5] For the NOM reference, the strongest peak at ~1720 cm^{-1} was likely from C=O bonding.[6] This peak shifted to 1610 cm^{-1} after reaction, indicating that the deprotonation of the carboxylate anion may be necessary in order to bond with iron(III) (hydr)oxides.[6] For the systems containing arsenate, the large peak in the Fe + As system at ~826 cm^{-1} is within the range of ~ 825-839 cm^{-1} in references for adsorbed arsenate on iron oxides.[7] The Fe + As + NOM system also has a single peak at ~829 cm^{-1} with no visible second peak, indicated monodentate complex formation for both system.[7]

X-ray absorption spectroscopy (XAS). XAS experiments were conducted at Beamline 13BM-D at the Advanced Photon Source (APS), Argonne National Laboratory, which utilizes a Si (111) monochromator. The focused X-ray beam size was 10 μm by 30 μm with a resolution of 1×10^{-4} ΔE/E and energy flux of 1×10^{9} at 10 keV. The As XANES K-edges was measured at 11.867 keV. XAS measurements were carried out under room temperature conditions for samples which were dried in a desiccator under ambient temperature and pressure.

X-ray absorption spectroscopy results also showed no differences between the two systems (Figure S5). XAS results show the formation of bidentate mono-nuclear (R ~ 2.5Å) and monodentate mononuclear (R ~ 3.7Å) As(V) complexation.[8] These XAS results may provide more accurate observations of the binding nature, because the bidentate peak is hard to observe using FTIR due to it being very close to the monodentate peak.

While the peaks for As(V) binding to iron were observed, we did not observe peaks form in XAS due to interactions between NOM and As(V). This may be due to drying effects. Both NOM and amorphous iron(III) (hydr)oxides are expected to contain significant quantities of water during GISAXS analysis. There is also water present during contact angle analysis, where the impact of As(V) on NOM was observed. Thus, due to drying effects, XAS could not give a complete picture of interactions between As(V) and NOM in our study.

In addition, previous studies have found that in the presence of NOM and iron, arsenic primarily associated with dissolved organic carbon through metal bridging with NOM-complexed iron.[9-15] Redman et al. tested arsenate complexation with six NOM samples using HPLC-ICP-MS analyses and found that, for the four NOM samples which formed arsenic-NOM complexes, the complexation extent correlated with iron content of the NOM sample.[16] Therefore, while NOM

interactions with arsenic can exist in our system, they may not be distinguishable using XAS if a larger fraction of As(V) is forming metal bridges with NOM-complexed iron.

In sum, *Ex situ* precipitate characterization using FTIR and XAS indicate that there are not significant differences between As-binding in the Fe(III) + As(V) system and Fe(III) + As(V) + NOM system. This is supported by both the XAS, where the spectra are nearly identical, and FTIR data, where there were no differences in the peak position from As(V) binding. Hence, changes in the nucleation and growth behavior stem from other physicochemical properties of precipitates, as described further in the main text of the manuscript.

References

1. Neil, C. W.; Lee, B.; Jun, Y.-S., Different Arsenate and Phosphate Incorporation Effects on the Nucleation and Growth of Iron (III)(Hydr) oxides on Quartz. *Environ. Sci. Technol.* **2014,** 48, (20), 11883-11891.
2. Hu, Y.; Lee, B.; Bell, C.; Jun, Y.-S., Environmentally abundant anions influence the nucleation, growth, ostwald ripening, and aggregation of hydrous Fe (III) oxides. *Langmuir* **2012,** 28, (20), 7737-7746.
3. Jun, Y. S.; Lee, B.; Waychunas, G. A., In situ observations of nanoparticle early development kinetics at mineral-water interfaces. *Environ. Sci. Technol.* **2010,** 44, 8182-8189.
4. Neil, C. W.; Lee, B.; Jun, Y. S., Different Arsenate and Phosphate Incorporation Effects on the Nucleation, Growth, and Formation Location of Iron(III) (Hydr)oxides on Quartz. *Envir. Sci. & Tech.* **2014,** 48, 11883-11891.
5. Wershaw, R. L.; Leenheer, J. A.; Cox, L. G. *Characterization of dissolved and particulate natural organic matter (NOM) in Neversink Reservoir, New York*; 2005.
6. Ferreira, Q.; Gomes, P. J.; Raposo, M.; Giacometti, J.; Oliveira, O. N.; Ribeiro, P. A., Influence of ionic interactions on the photoinduced birefringence of Poly [1-[4-(3-Carboxy-4 Hydroxyphenylazo) benzene sulfonamido]-1, 2-ethanediyl, sodium salt] films. *Journal of nanoscience and nanotechnology* **2007,** 7, (8), 2659-2666.
7. Guan, X.-H.; Wang, J.; Chusuei, C. C., Removal of arsenic from water using granular ferric hydroxide: macroscopic and microscopic studies. *J. Hazard. Mater.* **2008,** 156, (1), 178-185.
8. Manning, B. A.; Fendorf, S. E.; Goldberg, S., Surface structures and stability of arsenic (III) on goethite: spectroscopic evidence for inner-sphere complexes. *Environ. Sci. Technol.* **1998,** 32, (16), 2383-2388.

9. Ko, I.; Kim, J.-Y.; Kim, K.-W., Arsenic speciation and sorption kinetics in the As–hematite–humic acid system. *Colloids Surf. Physicochem. Eng. Aspects* **2004,** 234, (1), 43-50.
10. Lin, H.-T.; Wang, M.; Li, G.-C., Complexation of arsenate with humic substance in water extract of compost. *Chemosphere* **2004,** 56, (11), 1105-1112.
11. Warwick, P.; Inam, E.; Evans, N., Arsenic's interaction with humic acid. *Environmental Chemistry* **2005,** 2, (2), 119-124.
12. Ritter, K.; Aiken, G., R; Ranville, J. F.; Bauer, M.; Macalady, D. L., Evidence for the aquatic binding of arsenate by natural organic matter-suspended Fe (III). *Environ. Sci. Technol.* **2006,** 40, (17), 5380-5387.
13. Mikutta, C.; Kretzschmar, R., Spectroscopic evidence for ternary complex formation between arsenate and ferric iron complexes of humic substances. *Environ. Sci. Technol.* **2011,** 45, (22), 9550-9557.
14. Hoffmann, M.; Mikutta, C.; Kretzschmar, R., Arsenite binding to natural organic matter: spectroscopic evidence for ligand exchange and ternary complex formation. *Environ. Sci. Technol.* **2013,** 47, (21), 12165-12173.
15. Campbell, K. M.; Nordstrom, D. K., Arsenic speciation and sorption in natural environments. *Reviews in Mineralogy and Geochemistry* **2014,** 79, (1), 185-216.
16. Redman, A. D.; Macalady, D. L.; Ahmann, D., Natural organic matter affects arsenic speciation and sorption onto hematite. *Environ. Sci. Technol.* **2002,** 36, (13), 2889-2896.

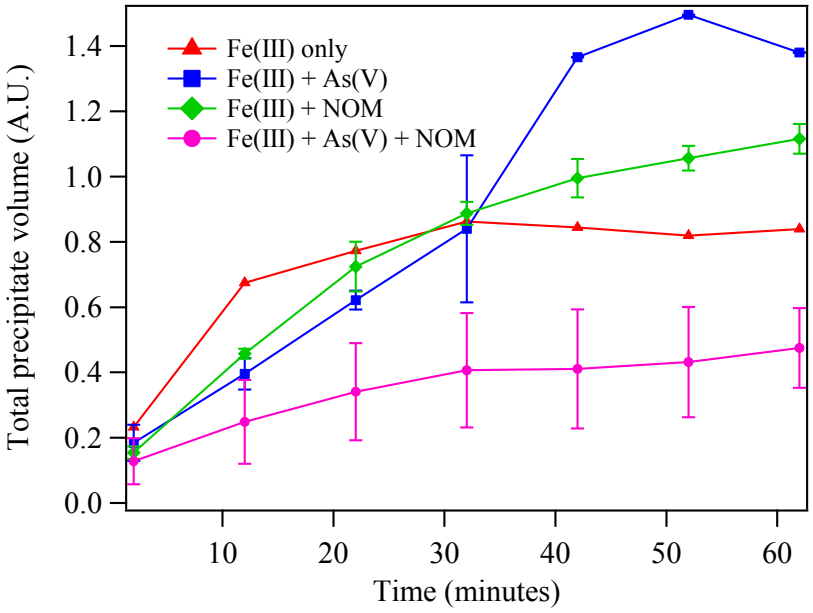

Figure S1. Total particle volume evolutions calculated from GISAXS scattering data. The pH for all systems was 3.6. All systems contained 10^{-4} M Fe(III). Systems with As(V) contained 10^{-5} M As(V) and systems with NOM contained 1.5 mg/L NPOC.

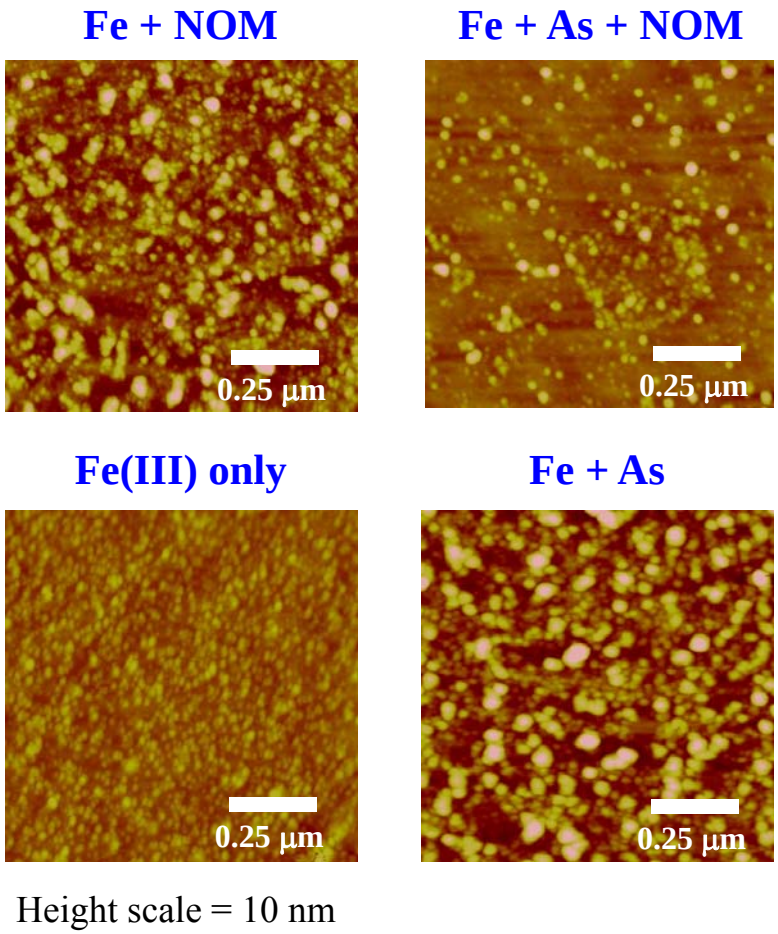

Figure S2. AFM images for the samples which were used in GISAXS experiments. Samples were reacted for 1 hour. The pH for all systems was 3.6. All systems contained 10^{-4} M Fe(III). Systems with As(V) contained 10^{-5} M As(V) and systems with NOM contained 1.5 mg/L NPOC.

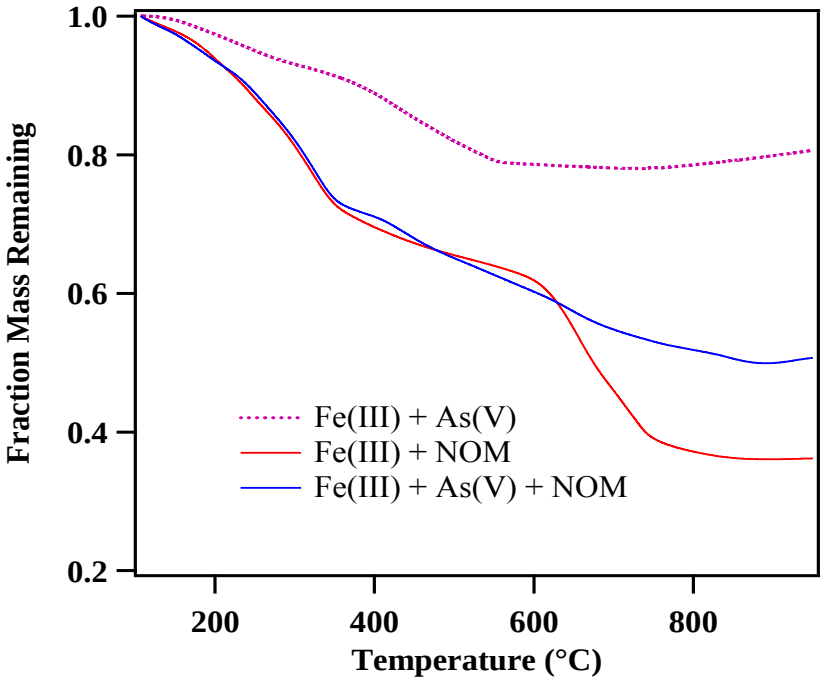

Figure S3. TGA data for experimental systems. The precipitates were collected after 1 hour. The pH for all systems was 3.6. All systems contained 10^{-4} M Fe(III). Systems with As(V) contained 10^{-5} M As(V) and systems with NOM contained 1.5 mg/L NPOC.

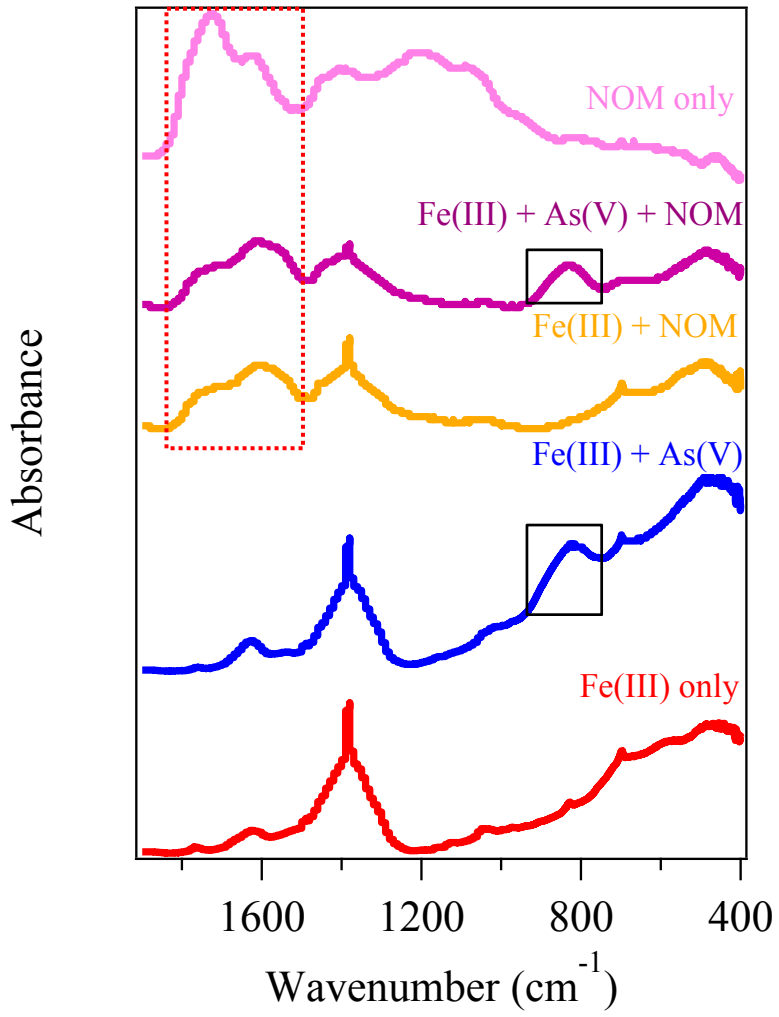

Figure S4. FTIR data for homogeneous precipitates in the four reaction systems show no differences in As and NOM binding to iron(III) (hydr)oxides. The red square indicates where peaks from NOM binding occur and the black squares indicate where As(V) is binding. The precipitates were collected after 1 hour. The pH for all systems was 3.6. All systems contained 10^{-4} M Fe(III). Systems with As(V) contained 10^{-5} M As(V) and systems with NOM contained 1.5 mg/L NPOC.

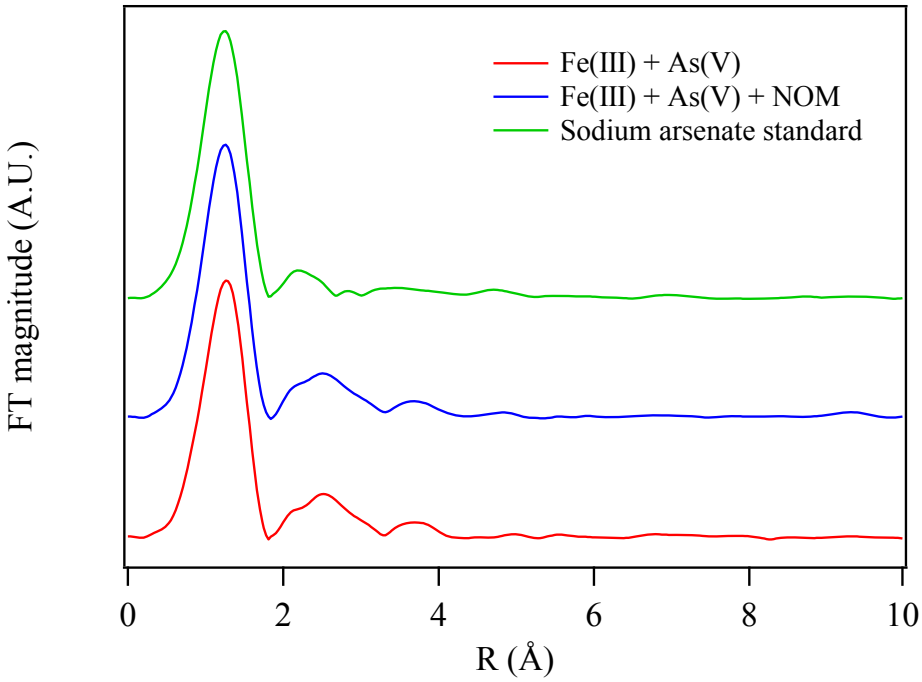

Figure S5. XAS Fourier transform data for As K-edge in reaction systems and sodium arsenate standard samples. The precipitates were collected after 1 hour. The pH for all systems was 3.6. All systems contained 10^{-4} M Fe(III). Systems with As(V) contained 10^{-5} M As(V) and systems with NOM contained 1.5 mg/L NPOC.

Table S1. Characterization of Suwannee River NOM provided by the IHSS.

Carboxyl (meq/g C)	Phenolic (meq/g C)	Q_1	pK_{a1}	n_1	Q_2	pK_{a2}	n_2	N	RMSE
11.21	2.47	11.20	4.16	3.44	1.60	9.99	1.03	1705	0.1360
Source: Department of Chemistry, Environmental Sciences Ph.D. Program, Ball State University, Muncie, IN, U.S.A.									
Q_1 and **Q_2** are the maximum charge densities of the two classes of binding sites **Log K_1** and **Log K_2** are the mean log K values for proton binding by the two classes of sites **n_1** and **n_2** are empirical parameters that control the width (in log K) of a class of proton binding sites									

Table S2. Time-resolved fractal dimensions for NOM-containing systems.

Time (minutes)	***Fe + NOM Fractal dimension***	***Fe + As + NOM Fractal dimension***
62	1.65	1.71
52	1.66	1.75
42	1.67	1.80
32	1.7	1.87
22	1.74	1.96
12	1.79	2.09
2	1.89	1.89